International Workshop on Atomic and Molecular Physics at High Brilliance Synchrotron Radiation Facilities, Hyogo, Japan, November 4-6, 1998

Precise tests of x-ray scattering theories in the Compton regime

B. KRÄSSIG, R. W. DUNFORD, D. S. GEMMELL, E. P. KANTER,
S. H. SOUTHWORTH, and L. YOUNG
Argonne National Laboratory
Argonne, Illinois 60439, USA
e-mail: kraessig@anl.gov

Abstract

We report two experiments intended to test the accuracy of state-of-the-art theoretical predictions for x-ray scattering from low-Z atoms. The first one deals with the differential x-ray scattering cross sections in Ne and He from 11–22 keV and the Ne Compton-to-Rayleigh scattering ratio in this energy range. It was found that, in order to be consistent with the experimental results, an accurate description at low Z must include nonlocal exchange, electron correlation, and dynamic effects. The second experiment concerns the ratio of helium double-to-single ionization for Compton scattering in the 8–28 keV energy range where published experimental and theoretical results so far fail to give a consistent picture. The progress of the experiment and the data analysis is reported.

1. Introduction

The importance of x-ray scattering as a tool in the study of material structures was recognized soon after Roentgen's discovery of x rays. With powerful modern x-ray synchrotron sources this tool is now being used in many different fields. Its applicability is based on a fundamental understanding of the process of x-rays scattering off electrons in the material. The interpretation of x-ray scattering data, both elastic and inelastic, relies on theoretical models of scattering processes. An improvement of instrumental sensitivity for finer detail requires therefore refinements in the theoretical description. The two experiments described in this progress report are aimed at providing precision tests for current state-of-the-art theoretical treatments of x-ray scattering from free atoms.

The subject of the first experiment is the scattering of x rays in neon and helium at 90 degrees from the the incident beam. In the energy range investigated, 11 to 22 keV, sizable differences exist between state-of-the-art relativistic S-matrix calculations and commonly used standard form factor calculations. In order to circumvent the large uncertainties encountered in absolute determinations of differential cross sections, we report the ratios of these cross sections for neon and helium and compare with the respective theoretical ratios. For the case of neon, where elastic Rayleigh scattering and inelastic Compton scattering are of similar magnitude in this energy range, a decomposition of the elastic and inelastic processes has been performed and the results are compared to theory. The findings of this experiment have recently been published [1].

DISCLAIMER

The second experiment deals with the subject of double ionization in helium by Compton scattering. Theoretical treatments of this case require the incorporation of electron correlation both in the initial bound state and in the final three-particle continuum state. Experimentally, this quantity is very difficult to determine because its cross section is very small. Published results in the energy range between the onset of Compton ionization up to 20 keV display substantial discrepancies in the energy dependence of the ratio $R_C = \mathrm{He}^{++}/\mathrm{He}^{+}$ for this process (cf. [2], and references therein). We measured R_C for x-ray energies between 8 keV and 28 keV [3]. This preliminary report describes details of the experiment and of the data analysis procedure.

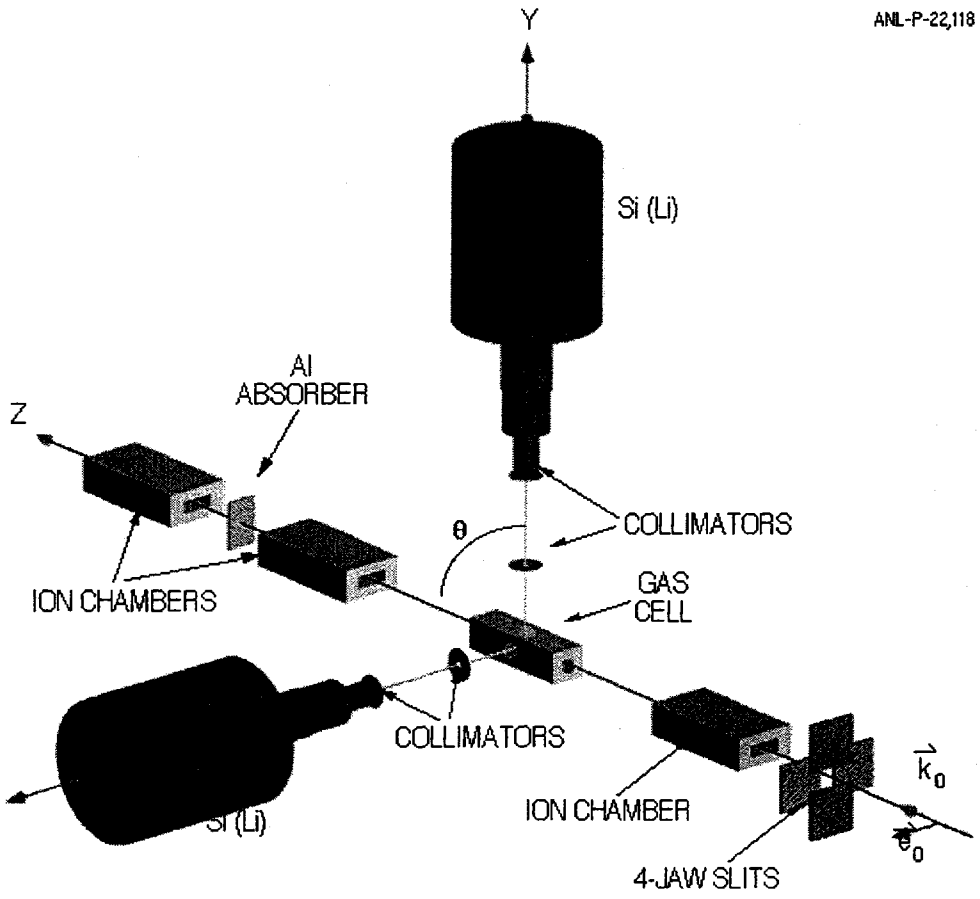

Figure 1: The experimental setup used in the x-ray scattering experiment.

2. Compton and Rayleigh Scattering in Neon and Helium

At present, even the more sophisticated theoretical treatments of the photon-atom scattering process are incomplete, treating either the interaction or the target atom accurately, but not both simultaneously. The nonrelativistic interaction Hamilitonian for the photon-electron system is $H_{\mathrm{int}} = \frac{e^2}{2mc^2}A^2 - \frac{e}{mc}\mathbf{p}\cdot\mathbf{A}$. Because scattering processes involve a photon in both the initial and final states, interaction matrix elements must include the vector potential, $\mathbf{A}$, quadratically. Con-

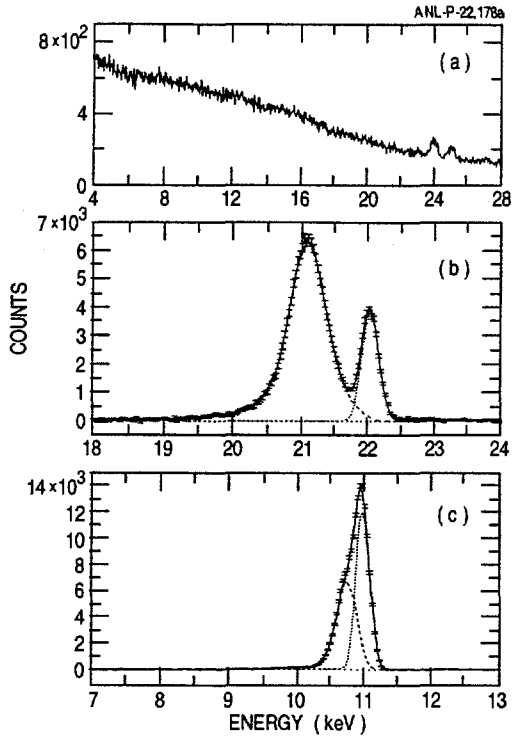

Figure 2: Energy spectra in the Si(Li) detector oriented normal to the polarisation plane. (a) Background spectrum with empty cell, (b) scattering from Ne at 22 keV, and (c) scattering from Ne at 11 keV. For (b) and (c) decomposition of the Compton and Rayleigh cross sections is shown in the dashed lines.

sequently, only the A^2 term contributes in first order and traditional calculations (see, e. g., [4]) have ignored the $\mathbf{p} \cdot \mathbf{A}$ term, describing the interaction in terms of user-friendly form-factors and incoherent scattering factors. In this manner, it is possible to include correlation in the description of the target atoms [5, 6, 7]. In contrast, numerical relativistic second-order S-matrix methods for elastic [8] and inelastic [9] scattering inherently include the full interaction, but simplify the target potential by using the independent particle approximation (IPA) and local exchange potentials. Due to the good overall agreement, particularly at higher Z, the S-matrix results have become accepted as benchmarks in elastic x-ray scattering calculations.

We measured differential cross sections at 90° scattering angle. The energies, 11, 15, 18, and 22 keV were chosen to lie far above the Ne K edge (870 eV) and in a region where Compton and Rayleigh scattering cross sections in neon are comparable. In the following, the differential cross sections at 90° for total, Compton, and Rayleigh scattering will be denoted at $d\sigma_{\mathrm{tot}}, d\sigma_C, d\sigma_R$. The results will be presented as ratios, $d\sigma_{\mathrm{tot}}(\mathrm{Ne})/d\sigma_{\mathrm{tot}}(\mathrm{He})$ and $d\sigma_C(\mathrm{Ne})/d\sigma_R(\mathrm{Ne})$. In this way several absolute measurements were circumvented, e.g., the determination of the x-ray flux and the detector efficiency. It should be noted that the elastic scattering channel in helium was well below the sensitivity of our experiment and that the observed photons originated pratically all from inelastic scattering. For the

cases of He and H_2 Ice *et al.* [10] found good agreement between experiment and theories which describe inelastic scattering in the impulse approximation (IA) and with correlated wavefunctions.

Our experiment was performed on a bending magnet beamline (12BM) at the Basic Energy Sciences Synchrotron Radiation Center (BESSRC) of the Advanced Photon Source (APS). Fig. 1 shows a schematic of the experiment. Monochromatized x rays were incident on the gas sample, creating a line source which was viewed simultaneously by two well-characterized Si(Li) detectors placed 90° about the photon beam propagation axis to eliminate the polarization dependence. Measurements were made at two pressures, 1 and 2 atm. Gas pressure was measured to $\approx 0.25\%$. The first, second, and third (with absorber) ion chambers were used for run-to-run normalization, measurement of the gas absorption, and measurement of the higher harmonic contribution in the beam, respectively.

Fig. 2 shows examples of the x-ray spectra recorded. Background measurements, shown in Fig. 2(a), were made by evacuating the cell. The two small features at 24 and 25 keV correspond to K_α emission from In and Sb impurities in the detector that were excited by scattered bremsstrahlung. Background measurements were made for all energies, scaled, and subsequently subtracted from the experimental spectra to produce the scattering spectra for He and Ne. Fig. 2(b) and (c) show scattered x-ray spectra for neon at 22 keV and 11 keV, respectively. The Compton and Rayleigh cross sections were separated using the well characterized detector response [11] and IA Hartree-Fock Compton profiles [12]. The fits are included in Figs. 2(b) and (c).

The results of our measurements are compared to the compiled results of theoretical predictions in Fig. 3. In the top panel the ratio $d\sigma_{\rm tot}({\rm Ne})/d\sigma_{\rm tot}({\rm He})$ is displayed; the neon Compton-to-Rayleigh ratios, $d\sigma_C({\rm Ne})/d\sigma_R({\rm Ne})$, are shown in the bottom panel. Because of their variation over the covered energy range and for an easier assessment of relative deviations, the data were normalized [13] to what in the following will be termed the 'best' prediction. The experimental data are shown as points with error bars. In top panel of Fig. 3 it can be noted that the full line ([4], representing nonrelativistic form-factor calculations for Rayleigh and incoherent scattering factor calculations for Compton) reproduces the experimental data for the total scattering ratio better than the squares, the prediction based on the S-matrix calculations (S-matrix for Rayleigh scattering and [4] for Compton). In contrast, the situation of agreement is reversed for the Compton-to-Rayleigh ratios in the bottom panel. The dot-dashed line results from the more sophisticated modified form-factor approach for Rayleigh scattering and includes the anomalous scattering factor (MFF+ASF); it reproduces the S-matrix results and shows the same discrepancies with the experimental values.

In order to understand the origins of these disagreements, the various approximations made in the different theoretical approaches were carefully examined in Ref. [1]. Here, we shall only present a brief sketch of this investigation. The starting point was a 'simplest' prediction, obtained from the form factor and impulse approximations and local nonrelativistic IPA bound state wavefunctions. In the 'best' prediction the 'simplest' has been perturbatively corrected for five effects: nonlocal exchange, electron correlation, relativity, dynamics, and Raman scattering. The most pronounced

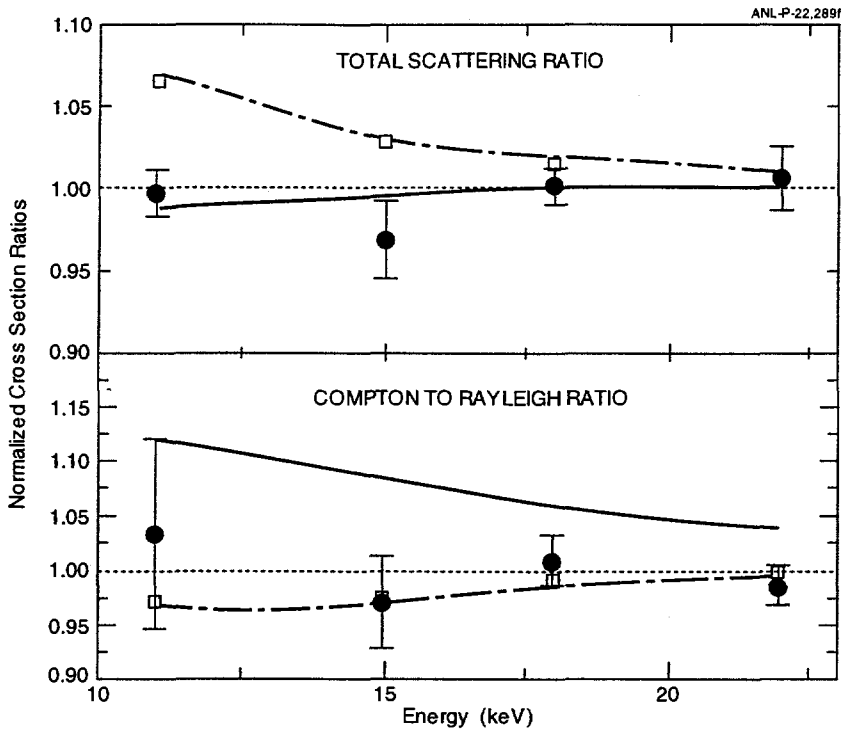

Figure 3: Top: Ratio of total scattering cross sections in neon to helium normalized to 'best' prediction. Bottom: Compton to Rayleigh cross section ratio. See text.

effects were found for Rayleigh scattering cross sections, where the use of nonlocal exchange versus local exchange changed the cross section by almost 10%. Both the S-matrix calculations and the MFF+ASF calculations use local exchange potentials. Refinement of the interaction dynamics, i.e. going beyond the standard form-factor approach caused a 5% change in the opposite direction. Electron correlation effects are more pronouced for Compton scattering at lower energies. It is clear that the partial compensation of these effects caused the contradictory situation encountered in the comparison of the experimental data to various theoretical calculations in Fig. 3. Using the 'best' prediction, the experimental data in both panels of Fig. 3 are reproduced within the error bars.

3. Double ionization of helium by Compton scattering

The experiment of Ice *et al.* [10] showed that the cross section for inelastic scattering of x rays in helium can be calculated to within a few percent. This finding, however, cannot be transferred to predictions for the partitioning of the total inelastic scattering into single and double ionization channels. The published theoretical and experimental results for the helium double-to-single ionization ratio by Compton scattering, R_C, are shown in Fig. 4. The three theories differ substantially in their predictions for x-ray energies up to 20 keV and the sparse experimental data don't allow a conclusive

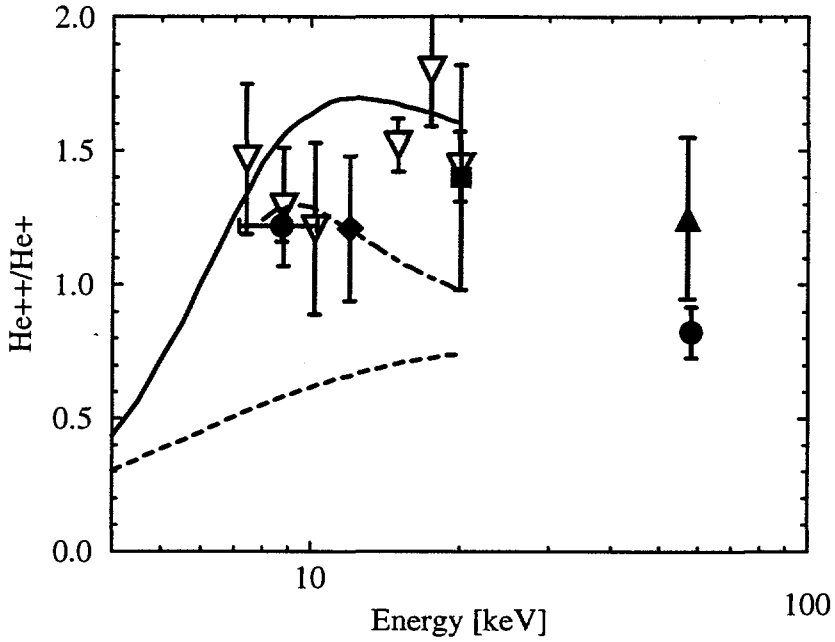

Figure 4: Published experimental and theoretical results on the ratio of double-to-single ionization in helium by Compton scattering. Solid circles, Refs. [2, 14]; open triangles, Ref. [15]; solid triangle, Ref. [17]; solid square, Ref. [16]; solid diamond, [18]; solid line Ref. [21]; dash-dotted line, Ref. [20]; dashed line, Ref. [19].

decision in favor of either one of these predictions (cf. [2]). The inherent difficulty for theoretical treatments lies in the proper description of electron correlation effects in both the initial and final states. In an attempt to circumvent part of this difficulty, only a correlated initial state wavefunction is needed for the IA calculation, however, the results of the IA prediction of double ionization seems to be least favored by the experiments [19]. Only in the limit of asymptotically high energies do the calculations become insensitive to the correlation in the final state. Mutual consistency between different theories has been reached for the asymptotic ratio $R_C^\infty \approx 0.8$ (cf. [22, 23]).

Experimental determinations of the helium double ionization ratio by Compton scattering are impeded by several difficulties. The cross section for Compton scattering is very small, 1 barn for single ionization, and double ionization amounts to about 1% of that. The vacuum requirements for single ion counting impose limitations on the target pressure in the interaction regime. Even though Compton scattering dominates in the ionization of helium above 6 keV, provisions have to be made to separate photoabsorption events from the Compton scattering events. Furthermore, because the the Compton cross section is many orders of magnitude smaller than electron impact cross sections, the experiment is highly sensitive to contaminating ionization events by secondary electrons created

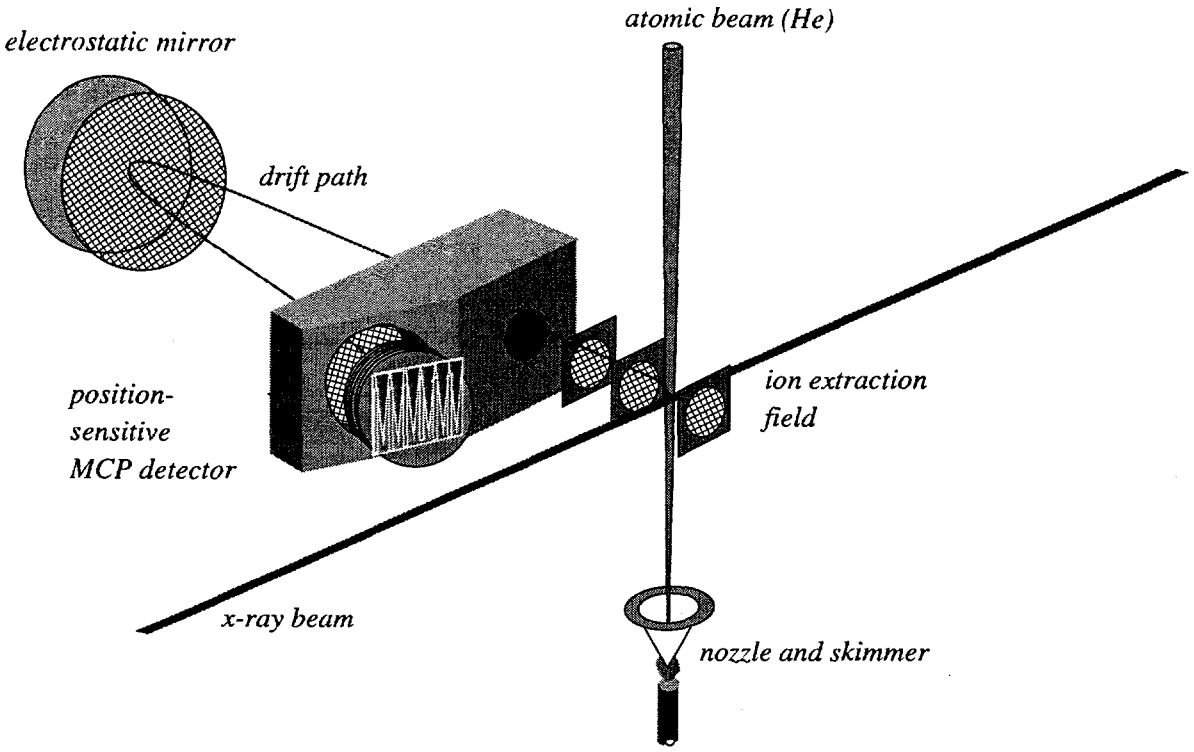

Figure 5: Schematic of the time-of-flight spectrometer.

along the beam path at windows, apertures, etc. Higher-order components in the x-ray beam may also influence the result. Special care must be taken to determine any differences in the transmission and detection efficiencies for the two helium charge states.

The experiment was performed at the BESSRC undulator beam line ID-12 at the Advanced Photon Source. The collimated x-ray beam (5×3 mm^2) entered and exited the vacuum chamber through 0.005" Be windows. The chamber was partitioned in three separately pumped stages for a skimmed supersonic jet arrangement. The jet diameter was about 5 mm in the interaction region. At 28 bar He backing pressure behind a 25 μm nozzle and with a 0.5 mm skimmer the target density in the interaction region was about 5×10^{12}cm^{-2}. The residual gas pressure in the chamber was 1×10^{-7} Torr.

A schematic of the Wiley-Mclaren-type time-of-flight (TOF) spectrometer is shown in Fig. 5. The total flight path is about 400 mm and includes a 160° reflection in an electrostatic mirror. The reflector virtually eliminates prompt counts on the detector caused by scattered x-rays and energetic electrons. The continuous extraction field was 177 V/cm, and the total acceleration potential between interaction region and the detector was 2900 V. The ratio of voltages in the interaction region and the neighboring acceleration region was optimized to achieve space focussing conditions. The detector consisted of a Z-stack MCP arrangement with a two-dimensionally position-sensitive wedge-and-strip anode.

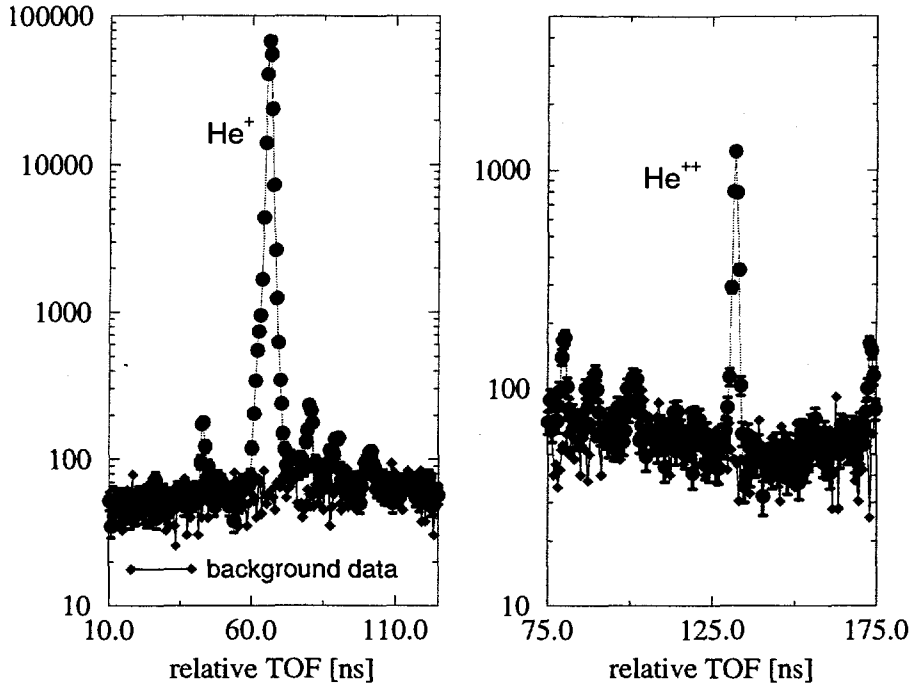

Figure 6: Compounded TOF spectra for He^+ (left) and He^{++} (right), measured at 16 keV.

In combination with the cooled jet of helium atoms, the position-sensitive detector, and event-mode data acquisition, the TOF spectrometer operates as a COLTRIMS system (Cold Target Recoil Ion Momentum Spectroscopy [24]). In our experiment the COLTRIMS technique is employed to separate photoabsorption events from Compton ionization events (cf. [14]): In a photoabsorption event the emitted photoelectron 'kicks' off the ion and the ion receives a measurable recoil momentum; in Compton scattering the photon undergoes a binary encounter with an atomic electron which couples only weakly to the ion through the binding forces. Following their extraction Compton ions travel through the TOF spectrometer on the centroid trajectory, whereas ions from photoabsorption are on transversely and/or longitudinally displaced trajectories. In addition to online monitoring of these parameters, the flight times and positions on the detector are individually recorded for each event and stored on tape for further analysis. Compton events are sorted out by properly selected software 'windows' in the detector image and the TOF spectrum.

The experiment utilized the timing operation mode offered at the APS. In this mode, termed '6+20 singlets', the positrons stored in the storage ring are distributed among the 1296 possible buckets in the following way (bucket spacing 2.8 ns): six filled buckets, 54 empty buckets, then 20 sequences of single filled buckets followed by 45 empty buckets. This fill patterns leaves 130.7 ns dark intervals between each of the 20 single bunch x-ray flashes, and one longer dark period of 1028 ns before the fill pattern repeats itself. An electronic signal synchronous to the fill pattern is provided.

The TOF of the He ions ($\approx 2\mu$s) is much longer than the 131 ns between bunches and consequently the TOF spectra of the 20 single bunches overlay each other. The extraction field was carefully chosen such that the TOF peaks belonging to the two charge states of helium didn't overlay each other. The twenty peaks for each charge state were subsequently added up into separate spectra. Examples of such compounded spectra are shown in Fig. 6. In the spectra shown in this figure only those events were accumulated which lay within a hexagonal window around the spot in the two-dimensional detector image corresponding to small transverse ion momenta. Data collection time per x-ray energy was typically 6–8 hours with target gas and additional 6–8 hours without target gas to determine the background in the spectra (also shown in Fig. 6). The smaller peak structures seen in the figure correspond to photoabsorption events with recoil momentum along the TOF axis, to a bunch impurity in the fill pattern five buckets after the single bunches, and to structure from residual gas ions.

The intersection of the x-ray beam with the jet of cold helium atoms creates a well-defined interaction region which, apart from transmission losses at four gold meshes, is imaged in its entirety onto the position-sensitive detector. In the offline data analysis great care was taken not to introduce discrimination of either one of the two charge states which could be caused by inadequate positioning of the software windows in the event sorting procedure. A selection of different window sizes and combinations in the detector images, the TOF spectra, and the detector pulse height spectra was used. It was verified that the result, within the statistical error, was the same for all of these window combinations.

The detection efficiency of MCPs for ions depends on their impact energies (cf. [25, 26]). The doubly charged He^{++} impinge on the MCP surface with twice the energy of the He^{+} ions. In a separate experiment with a pulsed electron gun using the same setup as in the x-ray experiment it has been determined that the detection efficiencies of He^{+} ions with 2900 eV and 5800 eV kinetic energy differed by $\approx 3\%$. All our ratio results have been corrected for this difference. In order to check that our apparatus was able to reproduce well-established results, we measured the ratio of helium double-to-single ionization by 5-keV electrons. We obtained $R_e(5\text{keV}) = 0.340(10)\%$ which is in agreement with the value published by Nagy *et al.* [25], $R_e(5\text{keV}) = 0.359(18)\%$.

X-ray measurements of the ratio R_C were made at six different energies, 8, 10, 13, 16, 20, and 28 keV. The results will be presented in a forthcoming paper [3]. Qualitatively, our measurements at 8 keV and 20 keV confirm the results published by Spielberger *et al.* [14] and Levin *et al.* [15] for the respective energies (cf. Fig. 4). In the energy dependence of R_C our results favor most the calculation by Bergstrom *et al.* [21] which lies about 10% above our data.

4. Summary

In this report we presented two experiments which accurately tested current theoretical predictions for x-ray scattering. In the first experiment we measured the total scattering at 90° (elastic

and inelastic) for helium and neon at 11–22 keV. It was found that none of the current theories for which numerical data are available can alone properly describe x-ray scattering in neon. The use of the standard form factor approach for Rayleigh and the IA for Compton clearly limits the accuracy of calculations. While the current IPA S-matrix theories for Rayleigh and Compton scattering are known to work well for high-Z elements and high energies, for low Z they are less reliable because they do not include nonlocal exchange and electron correlation effects. The second experiment dealt with measurements of the ratio of double-to-single ionization in helium by Compton scattering. Published theoretical predictions and previous experimental results display large discrepancies. The difficulty of theoretical approaches lies in the proper description of electron correlation, particularly in the final state. On the experimental side, the smallness of the cross section for Compton ionization presents the main obstacle. We reported on the progress of our new measurements of the ratio R_C at several energies between 8–28 keV using a COLTRIMS time-of-flight setup.

Acknowledgments

We are indebted to M. Jung, T. W. LeBrun, S. Hasegawa, J. P. J. Carney, L. LaJohn, R. H. Pratt, P. M. Bergstrom, Jr., T. Weber, W. Schmitt, and H. Schmidt-Böcking for their valuable contributions. We thank the BESSRC staff for assistance during the experiment. This work was supported by the U.S. Department of Energy, Office of Basic Energy Sciences, Chemical Sciences Division under Contract W-31-109-Eng-38.

References

[1] M. Jung *et al.*, Phys. Rev. Lett. **81**, 1596 (1998)

[2] L. Spielberger *et al.*, Phys. Rev. Lett. **76**, 4685 (1996)

[3] B. Krässig *et al.*, to be published

[4] J. H. Hubbell *et al.*, J. Phys. Chem. Ref. Data **4**, 471 (1975)

[5] E. M. A. Peixoto, C. F. Bunge, R. A. Bonham, Phys. Rev. **181**, 322 (1969)

[6] J. Wang, R. O. Esquivel, V. H. Smith, Jr., and C. F. Bunge, Phys. Rev. A **51**, 3812 (1995)

[7] H. Meyer, T. Müller, A. Schweig, Chem. Phys. **191**, 213 (1995); Acta Cryst. A **51**, 171 (1995)

[8] G. E. Brown, R. E. Peierls, and J. B. Woodward, Proc. Roy. Soc. London A **227**, 51 (1955); W. R. Johnson and F. D. Feiock, Phys. Rev **168**, 22 (1968); L. Kissel, R. H. Pratt, and S. C. Roy, Phys. Rev. A **22**, 1970 (1986)

[9] T. Surić *et al.*, Phys. Rev. Lett. **67**, 189 (1991); P. M. Bergstrom, Jr., *et al.*, Phys. Rev. A **48**, 1134 (1993)

[10] G. E. Ice, M. H. Chen, and B. Crasemann, Phys. Rev. A **17**, 650 (1978)

[11] R. Ali *et al.*, Phys. Rev A **55**, 994 (1997)

[12] F. Biggs, L. B. Mendelsohn, and J. B. Mann, At. Data Nucl. Data Tables **16**, 201 (1975)

[13] Unnormalized values can be found in Table I of Ref. [1]

[14] L. Spielberger *et al.*, Phys. Rev. Lett. **74**, 4615 (1995)

[15] J. C. Levin, G. B. Armen, and I. A. Sellin, Phys. Rev. Lett. **76**, 1220 (1996)

[16] J. A. R. Samson, Z. X. He, W. Stolte, and J. N. Cutler, J. Electr. Spectr. Rel. Phen. **78**, 19 (1996)

[17] R. Wehlitz *et al.*, Phys. Rev. A **53**, 3720 (1996)

[18] M. Sagurton, D. Morgan, and R. J. Bartlett, private communication

[19] T. Surić *et al.*, Phys. Rev. Lett. **73**, 790 (1994)

[20] L. R. Andersson and J. Burgdörfer, Phys. Rev. A **50**, R2810 (1994)

[21] P. M. Bergstrom, Jr., K. Hino, and J. Macek, Phys. Rev. A **51**, 3044 (1995)

[22] T. Surić, K. Pisk, R. H. Pratt, Phys. Lett. A **211**, 289 (1996)

[23] M. Kornberg and J. E. Miraglia, Phys. Rev. A **53**, R3709 (1996)

[24] J. Ullrich *et al.*, J. Phys. B: At. Mol. Opt. Physics **30**, 2917 (1997) Topical Review

[25] P. Nagy, A. Skutlartz, and V. Schmidt, J. Phys. B: At. Mol. Phys. **13**, 1249 (1980)

[26] B. Brehm *et al.*, Meas. Sci. Technol. **6**, 953 (1995)